Journal of Solid State Chemistry 183 (2010) 2451–2455

Contents lists available at ScienceDirect

Journal of Solid State Chemistry

journal homepage: www.elsevier.com/locate/jssc

Micro-Raman analysis of titanium oxide/carbon nanotubes-based nanocomposites for hydrogen sensing applications

S. Santangelo [a,*], G. Messina [a], G. Faggio [a], A. Donato [a], L. De Luca [a], N. Donato [b], A. Bonavita [c], G. Neri [c]

[a] Department of Mechanics and Materials, "Mediterranea" University of Reggio Calabria, I-89122 Reggio Calabria, Italy
[b] Department of Matter Physics and Electronic Engineering, University of Messina, I-98166 Messina, Italy
[c] Department of Industrial Chemistry and Materials Engineering, University of Messina, I-98166 Messina, Italy

ARTICLE INFO

Article history:
Received 14 June 2010
Received in revised form
9 August 2010
Accepted 10 August 2010
Available online 13 August 2010

Keywords:
Micro-Raman spectroscopy
Anatase
Carbon nanotube composites
Hydrogen sensors

ABSTRACT

Titanium oxide/carbon nanotubes-based nanocomposites (TiO_2/CNTs, prepared by sol–gel method, and 2%Pt/TiO_2/CNTs, obtained by wetness impregnation of the TiO_2/CNTs base material with a solution of platinum acetylacetonate) have been recently used as active layer in hydrogen sensing devices at near room temperature, obtaining quite different responsiveness. The microstructure of these hybrid materials is here systematically investigated by micro-Raman spectroscopy at 2.41 eV. The results show that regardless of the nominal C/Ti molar ratio (3.6 or 17.0) only the anatase phase of titania is formed. Theoretical calculations demonstrate that phonon confinement is fully responsible for the large blue-shift ($\sim$10 cm^{-1}) and broadening ($\sim$20 cm^{-1}) of the lowest-frequency Raman mode with respect to bulk anatase. The average size (4.3–5.0 nm) of TiO_2 crystallites, resulting from Raman spectra fitting, is in excellent agreement with those inferred from transmission electron microscopy and X-ray diffraction measurements.

1. Introduction

Growing interdisciplinary efforts are nowadays devoted to the development of hydrogen-fueled systems, whose safe use demands efficient hydrogen sensor devices. Several hybrid nanocomposites have been proposed as active materials for the fabrication of resistive sensors for detection of this gas down to very low concentration. A good response towards H_2 has been obtained by the use of nanostructured Pt (or Pd) on surface chemically oxidized CNTs [1,2]. Efficient RT hydrogen sensing devices have been prepared also by using Pt on TiO_2-nanotubes [3].

There is great interest also in detecting high concentration of H_2 in inert atmosphere, by means of devices operating at temperature as low as possible, preferably room temperature (RT). Recently, prototypes of sensors for monitoring high hydrogen concentration in inert environment at near RT have been realized employing Pt/TiO_2/CNTs as sensing layers [4].

Preliminary sensing tests have shown that, different from Pt/CNTs and TiO_2/CNTs, Pt/TiO_2/CNTs allow detection of H_2. This suggests the possibility that a synergic action among noble metal, titanium dioxide and nanotubes must be responsible for their sensing properties. In addition, the nominal C/Ti molar ratio is found to have a strong influence on responsiveness of the Pt/TiO_2/CNT-based sensors, while the thermal pretreatment in reducing ambient has positive effects on the sensor performance [4].

This paper deals with TiO_2/CNTs (prepared by sol–gel method), 2%Pt/CNTs and 2%Pt/TiO_2/CNTs (obtained by wetness impregnation). Aiming at evidencing the effects of platinum addition and thermal treatment on their microstructure, as well as of the nominal C/Ti molar ratio (3.6 or 17.0) on the crystallization phase of titania, a systematic micro-Raman spectroscopy (MRS) investigation is carried out on these hybrid materials. From the MRS study indications about the occurrence of relevant grain size effects emerge, which are discussed in the light of the complementary results obtained by transmission electron microscopy (TEM) and X-ray diffraction (XRD). The existence of any correlation between the results of spectroscopic analysis and sensing tests is further investigated.

2. Experimental

2.1. Nanocomposite preparation

In order to prepare CNT-based composites, CNTs are firstly functionalized by a treatment with concentrated nitric acid (15.8 N) at 110 °C for 18 h. TiO_2/CNTs composites with different nominal C/Ti molar ratios are prepared, by a sol–gel method, dispersing the functionalized CNTs in a solution of titanium isopropoxide in isopropanol previously held under reflux at 80 °C

* Corresponding author. Fax: +39 0965 875201.
E-mail address: saveria.santangelo@unirc.it (S. Santangelo).

0022-4596/$ - see front matter © 2010 Elsevier Inc. All rights reserved.
doi:10.1016/j.jssc.2010.08.018

for 1 h. Then the resulting suspension is stirred with a magnet for 3 h. Finally, the impregnated CNTs are separated from the solution by filtration.

Pt/CNTs and Pt/TiO_2/CNTs composites (Pt loading: 2 wt%) are obtained by wetness impregnation of the base materials with a solution of platinum acetylacetonate in acetone.

Before deposition on a ceramic substrate for sensor fabrication, the so-obtained composites are treated "in situ" at 200 °C for 2 h in a mixture of 5% H_2 in argon.

2.2. Nanocomposite analysis

Morphology of the obtained nanocomposites is investigated by TEM (JEOL JEM 2010, 200 kV, equipped with a Gatan 794 Multi-Scan CCD camera). Their crystalline structure is analyzed by measuring Raman scattering excited at 2.41 eV (514.5 nm). For this purpose, a microscope (Olympus BX40, X50 objective) coupled to a double monochromator (Jobin Yvon Ramanor U-1000) and a photomultiplier (Hamamatsu R943-02) operating in photon-counting mode is used. Care is taken to minimize heating of the sample by choosing low laser power (3 mW at its surface). An acquisition time of 30 s is used in order to obtain a sufficient S/N ratio. Spectra are recorded in the range 100–3350 cm^{-1} and normalized. Unless differently specified, Lorentzian bands, superimposed on a constant background, are used to fit the spectra. Center frequency, width (FWHM) and intensity of the bands are chosen by a least-square best-fit method using a commercially available spectroscopic analysis software package. The relative intensities are calculated as integrated-intensity ratios.

XRD patterns (Ital Structures APD 2000) are recorded using a Cu K_α radiation source. The 20–80° 2θ-angle range is analyzed in step scan mode (step: 0.02°, counting time: 1 s).

2.3. Sensing test

To fabricate the sensor device, a thick film is deposited by painting an aqueous paste of the composites synthesized on a ceramic substrate (alumina, $6 \times 3\ mm^2$ sized) supplied with comb-like Pt-electrodes and a Pt-heater. Before carrying out the sensing measurements, sensors are pre-treated "in situ" at different experimental conditions. Sensing tests are carried out in an apparatus interfaced with a personal computer. The apparatus consists of a stainless steel box (where the sensor is allocated), connected to gas supply (He and H_2) and power supply that allows fixing and controlling the working temperature (50 °C). The sensor response is defined as $S=100[(R-R_0)/R_0]$, where R_0 and R are the values of electrical resistance measured when the sensor is maintained under He- and H_2/He-flow (100 ml/min), respectively.

3. Results

TEM analysis [Fig. 1(a) and (b)] reveals that the titania does not uniformly coat CNTs. As shown in Fig. 1(a), both large agglomerate of small TiO_2 particles and isolated titania grains on CNTs are observed. The non-homogeneous structure of TiO_2/CNTs composites is schematized in Fig. 1(c), as reported by Yao et al. [5]. The dispersed TiO_2 nanoparticles [Fig. 1(b)] are likely

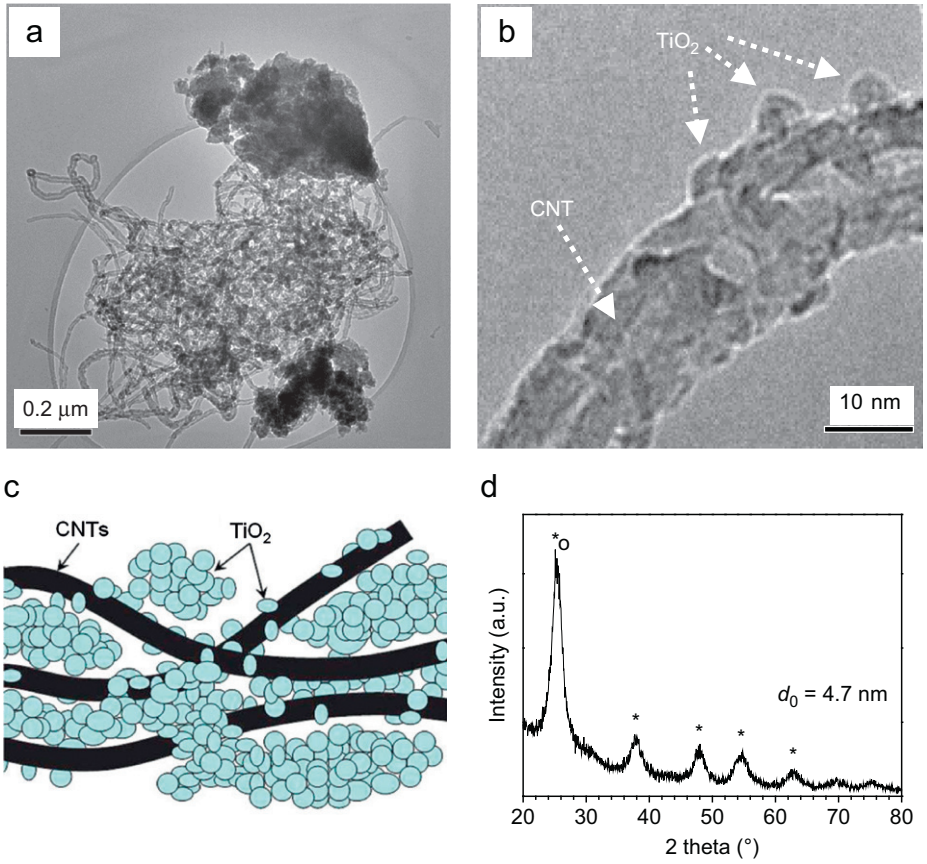

Fig. 1. (a, b) TEM images of TiO_2/CNTs composites and (c) schematic view of their non-homogeneous structure [5]. (d) XRD pattern of TiO_2/CNTs composites (the peaks originating from nanotubes and anatase phase of titania are marked with a circle and a star, respectively; average size d_0 of TiO_2 crystallites is also indicated). The shown TEM and XRD results refer to samples with 3.6 C/Ti molar ratio.

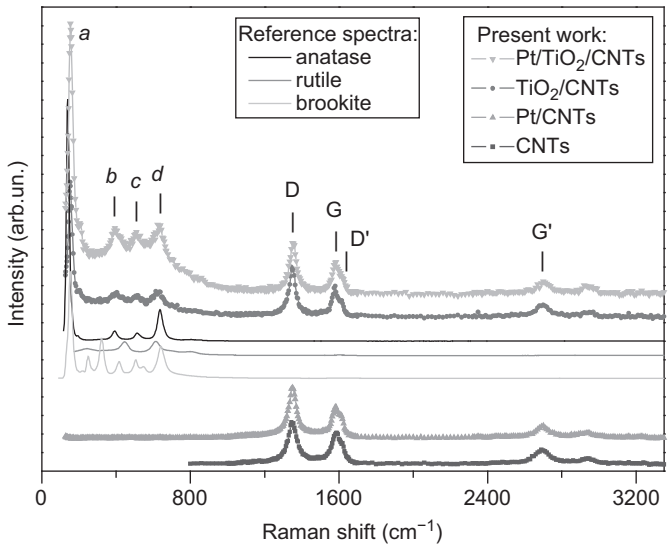

Fig. 2. Micro-Raman spectra of the materials investigated: pristine CNTs, binary (Pt/CNTs and TiO_2/CNTs) and ternary (Pt/TiO_2/CNTs) nanocomposites (all the spectra are normalized to the G-band intensity). The spectra of TiO_2/CNTs and Pt/TiO_2/CNTs refer to the case of C/Ti=3.6. Reference spectra of titania, as available in literature [10], are also shown.

anchored on carboxylic groups introduced during CNT surface functionalization. Their average size is estimated, using the Scherrer equation, from the XRD patterns [Fig. 1(d)].

Fig. 2 displays the MRS spectra of the investigated materials. The fingerprint of the graphitic crystalline arrangement (G-band at 1580 cm^{-1}, arising from the Raman allowed optical mode E_{2g} of graphite) and the disorder-activated (D and D′) bands, centered, respectively, at 1350 and 1610 cm^{-1} [6], are detected in all the spectra, together with the symmetry allowed D-band overtone (G′ band at 2700 cm^{-1}), indicative of long-range graphitic ordering. In addition, in the lower-frequency region (<1000 cm^{-1}) of the spectra of TiO_2/CNTs and Pt/TiO_2/CNTs, the features originating from the titania modes appear.

4. Discussion

4.1. Changes in crystalline structure of nanotubes

The introduction of –COOH groups by acid treatment brings about an increase of structural disorder in the graphitic lattice [2,7], which is revealed by the enhancement of D/G intensity ratio (from 1.4 in as-purchased CNTs up to 1.6 in the functionalized CNTs).

In hybrid nanocomposites, the disorder level further augments owing to the presence of metal and/or oxide nanoclusters, preferentially formed at defect sites of the pristine CNTs or attached to functional groups of the chemically oxidized CNTs [2,7] (D/G ratio increases up to 1.8 in Pt/CNTs, and up to 2.0 in TiO_2/CNTs and Pt/TiO_2/CNTs).

No further relevant changes are observed in the region (>1000 cm^{-1}) of Csp^2 vibration modes of the spectra (Fig. 2).

4.2. Phase of titanium oxide

As known [8], titania crystallizes in three phases: rutile (tetragonal), anatase (tetragonal) and brookite (orthorhombic), which exhibit quite different Raman fingerprints (Fig. 2).

Regardless of the nominal C/Ti molar ratio (3.6 or 17.0), four main spectral features (*a*–*d* in Fig. 2) are clearly visible in the spectra of TiO_2/CNTs and Pt/TiO_2/CNTs, centered approximately at 153, 398, 515 and 632 cm^{-1}, respectively. Comparison with frequency positions and relative intensities of titania reference spectra [9], available in Raman libraries [10], evidences a marked similarity with the spectrum of anatase. Hence, it is concluded that, even if the presence of smaller amounts of rutile and/or brookite cannot be in principle ruled out, anatase is the phase mainly present in titania nanoclusters of the hybrid composites under study.

Actually, the peaks detected in the XRD patterns of TiO_2/CNTs [Fig. 1(d)] indicate that nanocrystalline anatase phase is solely formed.

4.3. Nanostructure of titanium oxide

Anatase structure belongs to the space group D_{4h} ($I4_1/amd$) and contains two formula units per primitive unit cell [8,11]. According to the group analysis, there are six Raman active modes, $A_{1g}+2B_{1g}+3E_g$, located at 144 cm^{-1} (E_g), 197 cm^{-1} (E_g), 399 cm^{-1} (B_{1g}), 513 cm^{-1} (A_{1g}), 519 cm^{-1} (B_{1g}) and 639 cm^{-1} (E_g) [12].

In the present case, all the spectral features are broadened and/or shifted with respect to anatase bulk (Fig. 2). The largest differences concern the highest and the lowest frequency E_g modes. The former is red-shifted (at 633 cm^{-1}), while the latter, blue-shifted and broadened (of $\sim$10 and $\sim$20 cm^{-1} relative, respectively, to position and FWHM of the peak in bulk anatase), exhibits considerable asymmetry on the high-frequency side. Moreover, the spectra decomposition reveals that titania features are superimposed to a quite broad Gaussian band [Fig. 3(a)].

Grain-size-dependent variations in the Raman spectrum have been reported both for rutile [13] and anatase phases [14,15,17] of TiO_2 nanocrystals.

The average size (d_0) of titania crystallites in the present composites is estimated from the XRD patterns [Fig. 1(d)]. Since the most intense (1 0 1) peak of anatase ($2\theta \cong 25.4^\circ$) is partly superimposed to the CNT signal ($2\theta \cong 26.3^\circ$), the Gaussian (2 0 0) peak at $2\theta = 48.0^\circ$ is used for the estimation, obtaining values of the order of 5 nm, in full agreement with TEM observations [Fig. 1(b)].

In order to ascertain whether, and to what extent, phonon confinement effects are responsible for the blue-shift and broadening observed, profile of the E_g peak arising from external vibration of the anatase structure [14] has been calculated [Fig. 3(b)].

As known, in nanocrystals finite-size effects break the basic translational symmetry and relax the phonon momentum selection rule ($q \approx 0$), causing also the off-center phonons to contribute to the first-order Raman scattering. The weight of their contribution increases with decreasing crystallite size (d). The phonon dispersion causes asymmetric broadening and shift of the Raman lines.

The first-order Raman scattering intensity can be written as

$$I(\omega) = \int_{BZ} \frac{|C(0,q)^2| d^3q}{[\omega - \omega(q)]^2 + (\Gamma_0/2)^2}, \quad (1)$$

where $\omega(q)$ is the phonon dispersion curve and Γ_0 (7 cm^{-1} for the bulk anatase [16]) is the natural Raman linewidth at RT. A Gaussian weighting function

$$\left|C(0,q)^2\right| = \exp\left(\frac{-q^2 d^2}{16\pi}\right)$$

is generally used to model scattering away from the zone center [14] for spherical nanocrystals having diameter d.

Since experimental dispersion data for the anatase phase are not available, in order to calculate broadening and shift of the

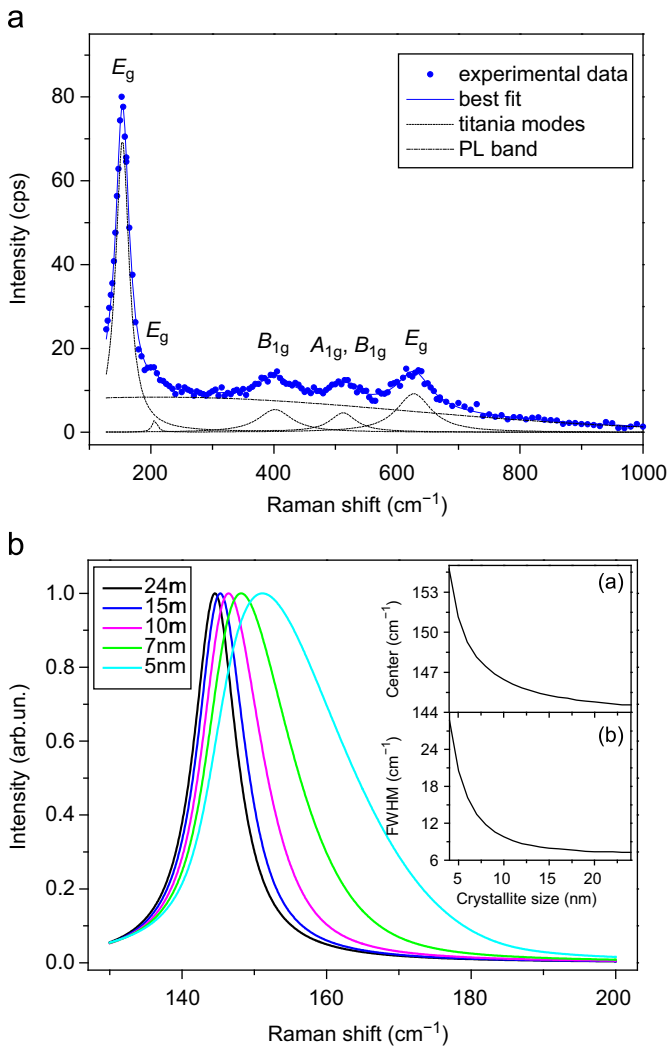

Fig. 3. (a) Region of titania vibration modes in micro-Raman spectrum of TiO_2/CNTs (in the case shown C/Ti is 3.6). (b) Profiles of the band arising from the lowest-frequency E_g mode of anatase titania, calculated in the phonon confinement model for different crystallite sizes. The inset shows the calculated center frequency position (a) and FWHM (b) of the E_g band as a function of crystallite size.

Raman peak from Eq. (1), the theoretical $\omega(q)$ curve [16] is used:

$$\omega(q) = \Delta[1\text{-}\cos(qa)] + \omega_0,$$

with $\Delta = 20\ \text{cm}^{-1}$ and $\omega_0 = 144\ \text{cm}^{-1}$ [14]. The results, obtained by considering a spherical Brillouin zone (BZ) with a diameter of $2\pi/a$ ($a = 0.3768$ nm being the anatase lattice parameter), are shown in Fig. 3(b). For $d \leq 15$ nm, grain size effects become important, causing remarkable band asymmetry, broadening and blue-shift. The calculated FWHM and frequency position of the E_g band are shown in the inset of Fig. 3(b) as a function of crystallite size.

The d_0 values, obtained by fitting the experimental data, fall in the range 4.3–5.0 nm, in excellent agreement with those inferred from the XRD patterns. Hence grain size is fully responsible for the band asymmetry, broadening and shift, which allows ruling out the involvement of other mechanisms, such as non-stoichiometry [14] and sample heating by laser irradiation.

4.4. *Effects of C/Ti molar ratio, platinum addition and reducing treatment*

Under laser irradiation in the visible range (2.41–2.71 eV), anatase nanopowders display strong visible light emission [18].

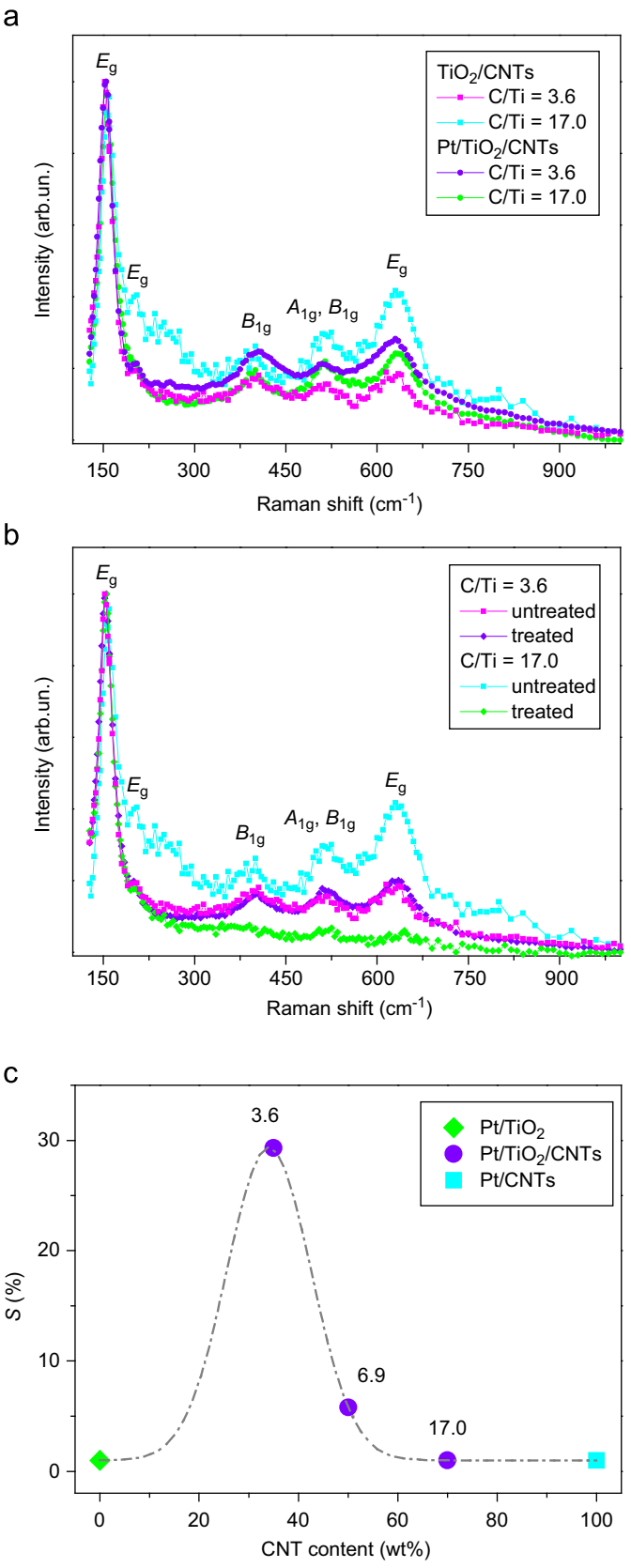

Fig. 4. Effect of (a) change of C/Ti molar ratio and platinum addition and of (b) reducing pretreatment in TiO_2/CNTs. All the spectra are normalized to the E_g-band intensity. (c) Change in responsiveness (S), measured at an operating temperature of 50 °C, with varying CNT content of active layer is also shown (for Pt/TiO_2/CNTs the corresponding C/Ti ratio is indicated; a line is drawn to guide the eyes).

As ascertained by performing measurements at different excitation energies (2.71 eV), in the spectra of all the investigated TiO_2/CNTs and Pt/TiO_2/CNTs, the anatase vibration modes are superimposed to a photoluminescence (PL) band with center energy position around 2.35 eV (444 cm^{-1}) [Fig. 4]. Three mechanisms (self-trapped excitons, surface states and oxygen vacancies) have been proposed [18] to explain the origin of PL in anatase nanopowders.

Clarifying the physical origin of the band observed here needs further investigations and is, hence, out of the aims of present work (for this purpose, new runs of PL measurements are currently in progress). However, it is interesting to note that in untreated TiO_2/CNTs, with increasing C/Ti molar ratio from 3.6 to 17.0, the lowest-frequency Raman mode further blue-shifts and broadens with respect to bulk anatase, signaling that TiO_2 grain size becomes smaller. For C/Ti=17.0, d_0=4.3 nm is obtained both by fitting the quite asymmetric E_g peak and applying the Scherrer formula to XRD data. These changes are accompanied by an increase of PL band intensities (relative to the lowest-frequency E_g mode) and by the appearance of an additional band [Fig. 4(a)] in the region (240–290 cm^{-1}), where the contribution due to lattice disorder or oxygen vacancies is usually reported [11,14].

Battiston et al. [17] have recently reported that a gradual increase in crystallite size is obtained in thin TiO_2 films by annealing in air at increasing temperatures. Spectral variations opposite to those observed here (namely, reduction in bandwidth of the anatase E_g mode and its red-shift) qualitatively confirm the improvement in film crystallinity. The decrease of relative intensity of the cathodo-luminescence band located at 610 nm further reveals that oxygen vacancy concentration in titanium oxide also progressively reduces as a consequence of the annealing.

These results support the conclusion that, in the present case, increase of C/Ti molar ratio favors decrease of crystallinity and the formation of a smaller-sized, more structurally disordered and/or less stoichiometric anatase phase, further hinting at the possibility that oxygen vacancies may be the origin of the PL located at 2.35 eV.

For C/Ti=17.0, the band in the 240–290 cm^{-1} region disappears and PL/E_g intensity ratio lowers both after Pt addition [Fig. 4(a)] and reducing treatment [Fig. 4(b)]. Contrarily, for C/Ti=3.6, the relative PL intensity enhances after Pt addition [Fig. 4(a)], while it does not undergo relevant changes after reducing treatment [Fig. 4(b)].

By comparatively examining the changes produced on PL by variation of C/Ti molar ratio, Pt addition and reducing pretreatment [Figs. 4(a) and (b)] and the results of sensing test [4], interesting details come into view.

Preliminary sensing tests have shown that only Pt/TiO_2/CNTs allow detection of H_2; such behavior can be interpreted on the basis of an exclusive synergic action, requiring the simultaneous presence of all composite components. The nature of thermal treatment (temperature, time, atmosphere composition) is another factor influencing the sensing properties of the composite. Indeed, it has been demonstrated that the sensor baseline becomes more stable if the active material is pre-treated in reducing ambient [4]. In order to find the optimal composition and establish correlations between sensing, microstructural and electrical properties, sensor response vs. nominal MWCNT loading in the composite has been investigated. It has been established that the responsiveness enhances with decreasing C/Ti ratio [Fig. 4(c)], showing a maximum at C/Ti=3.6 [4]. The calibration curve of this latter composite-based sensor highlights the satisfactory linearity of the sensing film in a wide range of hydrogen concentration, as required for near RT operating hydrogen sensors in inert environments.

The results of present investigation show that a variation of the relative PL/E_g intensity (i.e. a change of radiative to non-radiative recombination probability) is associated with all the factors (Pt addition, decrease of C/Ti ratio and pretreatment in H_2/Ar) having positive impact on sensor performance.

5. Conclusion

Systematic investigation of the microstructure of TiO_2/CNTs hybrid materials by MRS at 2.41 eV evidences that independent of the nominal C/Ti molar ratio (3.6 or 17.0) titania crystallizes in the anatase phase. The increase of C/Ti promotes diminishing of grain size and favors lattice disorder and/or non-stoichiometry at the expense of anatase crystallinity. Theoretical calculations demonstrate that phonon confinement is fully responsible for the large blue-shift ($\sim$10 cm^{-1}) and broadening ($\sim$20 cm^{-1}) of the lowest-frequency Raman mode with respect to bulk anatase.

A photoluminescence band centered approximately at 2.35 eV is detected in the spectra of all the investigated TiO_2/CNTs and Pt/TiO_2/CNTs. Although further work is needed to clarify its origin, it is found that a variation of its intensity, relative to the strongest TiO_2 Raman mode, is associated with all the factors – Pt addition, decrease of C/Ti ratio and pretreatment in H_2/Ar – improving sensor performance.

References

[1] M. Krishna Kumar, S. Ramaprabhu, J. Phys. Chem. B 110 (2006) 11291–11298.
[2] M. Krishna Kumar, S. Ramaprabhu, Int. J. Hydrogen Energy 32 (2007) 2518–2526.
[3] O.K. Varghese, D. Gong, M. Paulose, K.G. Ong, C.A. Grimes, Sensors Actuators B 93 (2003) 338–344.
[4] L. De Luca, A. Donato, G. Apa, S. Santangelo, G. Faggio, G. Messina, N. Donato, A. Bonavita, G. Neri, AISEM2010 Conference Proceedings, Messina, Italy, 8–11 February 2010.
[5] Y. Yao, G. Li, S. Ciston, R.M. Lueptow, K.A.G. Ray, Environ. Sci. Technol. 42 (2008) 4952–4957.
[6] M.S. Dresselhaus, G. Dresselhaus, R. Saito, A. Jorio, Phys. Rep. 409 (2005) 47–99.
[7] C.C. Chen, C.F. Chen, C.M. Chen, F.T. Chuang, Electrochem. Commun. 9 (2007) 159–163.
[8] L. Qian, Z.L. Du, S.Y. Yang, Z.S. Jin, J. Mol. Struct. 749 (2005) 103–107.
[9] Y. Hu, H.L. Tsai, C.L. Huang, J. Eur. Ceram. Soc. 23 (2003) 691–696.
[10] 〈http://rruff.info/〉.
[11] M.A. Khan, H.T. Jung, O.-B. Yang, Chem. Phys. Lett. 458 (2008) 134–137.
[12] S.W. Lu, C. Harris, S. Walck, M. Arbab, J. Mater. Sci. 44 (2009) 541–544.
[13] V. Swamy, B.C. Muddle, Q. Dai, Appl. Phys. Lett. 89 (2006) 163118–163120.
[14] W.F. Zhang, Y.L. He, M.S. Zhang, Z. Yin, Q. Chen, J. Phys. D 33 (2000) 912–916.
[15] W.F. Zhang, M.S. Zhang, Z. Yin, Q. Chen, Appl. Phys. B 70 (2000) 261–265.
[16] D. Bersani, P.P. Lottici, X.Z. Ding, Appl. Phys. Lett. 72 (1998) 73–75.
[17] S. Battiston, A. Leto, M. Minella, R. Gerbasi, E. Miorin, M. Fabrizio, S. Daolio, E. Tondello, G. Pezzotti, J. Phys. Chem. A 114 (2010) 5295–5298.
[18] M. Šćepanović, Z.D. Dohčević-Mitrović, I. Hinić, M. Grujić-Brojčin, G. Stanišić, Z.V. Popović, Mater. Sci. Forum 494 (2005) 265–270.